

# Optimal Control for Maximizing Link Velocity of Visco-elastic joints

Mehmet Can Özparpucu and Sami Haddadin

**Abstract**—Designing intrinsically elastic robots recently attracted significant attention. Inspired by the elasticity in biological muscles, these designs aim at enabling robots to imitate human or animal motions during various tasks such as hopping, running, etc. In particular, reaching peak velocities, using the stored energy in the according elasticities, is of great interest. Applying optimal control theory, we investigate the problem of maximizing link velocity for visco-elastic joints. The main contribution of the paper is thus isolating the effects of mechanical joint damping on the optimal control policy.

## I. INTRODUCTION

Actuators with passive compliance are becoming extremely popular [15]. Two major properties of these actuators are their ability to absorb shocks and to store potential energy in their elastic elements. Exploiting these properties in order to realize highly dynamic motions that could not be achieved with rigid robots is our main goal. In particular, the energy storage ability of visco-elastic joints may result in a significant performance increase. A recent implementation of such a robot is the DLR Hand-Arm System [4], which is shown to be capable of outperforming classical rigid robots in throwing motions [8]. In this paper, we focus on maximizing the performance of a visco-elastic joint in terms of its maximally achievable link velocity. The solution to this problem was already discussed in [9] for a 1-DoF<sup>1</sup> undamped elastic joint. The same system was then investigated further in the presence of a deflection constraint by solving a minimum time problem to reach the maximum velocity [5]. The results were then extended to general undamped VSA joints [7], [8], [10] with experiments verifying that the obtained optimal controls are applicable to real systems. In this line of research, the present paper discusses how mechanical joint damping influences the optimal strategy to maximize the link velocity of a 1-DoF visco-elastic joint and investigates the maximum performance limit imposed by the according joint dynamics.

The paper is organized as follows. Section II gives a concise introduction to Optimal Control (OC) theory with particular focus on the Minimum Principle. In Section III, OC is applied to a 1-DoF visco-elastic joint robot for different motor models. Optimal control strategies are found, which are interpreted in terms of the system's impulse response functions and used to find maximum performance of visco-elastic joints, i.e. the joint speed gain. The obtained results are validated with numerical simulations in Section IV.

## II. OPTIMAL CONTROL AND THE MINIMUM PRINCIPLE

The objective of this paper is to derive and discuss optimal control strategies, which exploit intrinsic elasticity for reaching peak link side velocities. The main mathematical tool used for the derivation of these strategies is Optimal Control (OC) theory and the Minimum Principle [11], [13]. In this section we summarize some results of the Minimum Principle, which are used in the paper.

<sup>1</sup>DoF:degree of freedom

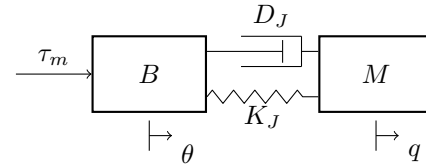


Fig. 1: 1-DoF Visco-Elastic Joint

For a dynamical system described by first order differential equations  $\dot{x} = f(x, u, t)$ , the Minimum Principle provides necessary conditions to be satisfied by the optimal control  $u^* \in \mathbb{U} \subset \mathbb{R}^m$ , which minimizes the following scalar-valued cost functional  $J(u)$ :

$$J(u) = \vartheta(x(t_f), t_f) + \int_{t_0}^{t_f} L(x, u, t) dt. \quad (1)$$

In (1),  $L$  is called the running cost,  $\vartheta$  the terminal cost,  $t_f$  the final time, and  $x \in \mathbb{R}^n$  denotes the system states [11]. The function space, to which the control trajectories  $u$  belong and over which the minimization takes place, will be the space of piecewise continuous functions  $PC^0$ . The differential equations  $f(x, u, t)$  are assumed to have a unique solution for  $t \in [t_0, t_f]$  and the set  $\mathbb{U} \subset \mathbb{R}^m$ , which the controls  $u$  belong to, will depend only on time or remain constant otherwise. Under these assumptions, the Minimum Principle states that the optimal control  $u^*$  minimizing the cost functional (1) also minimizes the Hamiltonian  $\mathbb{H}$  on the optimal trajectory at every time instant  $t \in [t_0, t_f]$ :

$$(\forall u \in \mathbb{U})[\mathbb{H}(x^*, \lambda^*, u^*, t) \leq \mathbb{H}(x^*, \lambda^*, u, t)], \quad (2)$$

where the Hamiltonian  $\mathbb{H}$  is defined as:

$$\mathbb{H} := \lambda^T f + L. \quad (3)$$

The dynamics of the optimal costates  $\lambda^*$  in (2) are determined in terms of  $\mathbb{H}$ :

$$\dot{\lambda}^* = - \left. \frac{\partial \mathbb{H}}{\partial x} \right|_*, \quad (4)$$

and if no terminal constraints are present, the following transversality condition holds at final time  $t_f$ :

$$\lambda^*(t_f) = \left. \frac{\delta \vartheta}{\delta x} \right|_{t_f, x_f^*} \quad (5)$$

The condition on the Hamiltonian along the optimal trajectory (2) will be of great importance in determining the optimal strategies for the discussed joints.

## III. VISCO-ELASTIC JOINTS

The 1-DoF robot joint with constant joint stiffness  $K_J$  and damping  $D_J$ , which we discuss in this paper is depicted in

Excitation $u_1$	$u_1 = \dot{\theta}$	$u_1 = \ddot{\theta}$	$u_1 = \tau_m/B$
States $\mathbf{x}$	$\begin{pmatrix} \phi \\ \dot{q} \end{pmatrix}$	$\begin{pmatrix} x_1 \\ x_2 \\ x_3 \end{pmatrix} = \begin{pmatrix} \phi \\ \dot{q} \\ \ddot{\theta} \end{pmatrix}$	$\begin{pmatrix} x_1 \\ x_2 \\ x_3 \end{pmatrix} = \begin{pmatrix} \phi \\ \dot{q} \\ \dot{\theta} + \alpha \dot{q} \end{pmatrix}$
Differential Equations $\mathbf{f}(\mathbf{x}, u_1)$	$\begin{pmatrix} u_1 - x_2 \\ \omega^2 x_1 + 2D\omega(u_1 - x_2) \end{pmatrix}$	$\begin{pmatrix} x_3 - x_2 \\ \omega^2 x_1 + 2D\omega(x_3 - x_2) \end{pmatrix}$	$\begin{pmatrix} x_3 - (\alpha + 1)x_2 \\ \omega^2 x_1 + 2D\omega(x_3 - (\alpha + 1)x_2) \end{pmatrix}$
Costates $\dot{\lambda} = -\frac{\partial \mathbb{H}}{\partial \mathbf{x}} = -\frac{\partial(\lambda^T \mathbf{f}(\mathbf{x}, u_1))}{\partial \mathbf{x}}$	$\begin{pmatrix} -\omega^2 \lambda_2 \\ \lambda_1 + 2D\omega \lambda_2 \end{pmatrix}$	$\begin{pmatrix} -\omega^2 \lambda_2 \\ \lambda_1 + 2D\omega \lambda_2 \\ -\lambda_1 - 2D\omega \lambda_2 \end{pmatrix}$	$\begin{pmatrix} -\omega^2 \lambda_2 \\ (\alpha + 1)(\lambda_1 + 2D\omega \lambda_2) \\ -\lambda_1 - 2D\omega \lambda_2 \end{pmatrix}$

TABLE I: OC Problems for the Unconstrained Elastic Joint with Constant Stiffness

$$\omega^2 = \frac{K_J}{M}, D = \frac{D_J}{2\sqrt{K_J M}}, \alpha = \frac{M}{B}, J(u_1) = -x_2(t_f)$$

Fig. 1. The linear differential equations describing the link and motor dynamics are of second order:

$$M\ddot{q} + D_J\dot{q} + K_Jq = K_J\theta + D_J\dot{\theta} \quad (6)$$

$$B\ddot{\theta} + D_J\dot{\theta} + K_J\theta = K_Jq + D_J\dot{q} + \tau_m, \quad (7)$$

where  $q$  denotes the link position,  $\theta$  the motor position,  $M$  the link inertia,  $B$  the motor inertia, and  $\tau_m$  the motor torque. We want to compute control strategies that maximize the final link velocity  $\dot{q}(t_f)$  at final time  $t_f$ . The corresponding cost functional  $J$  to be minimized then takes the form

$$J = \vartheta(t_f) = -\dot{q}(t_f). \quad (8)$$

Note that this cost functional does not consist of any running costs, which are usually included to ensure that constraints on the real system are not violated. However, since we want to obtain the optimal strategy that fully exploits the system dynamics, we first turn our attention to the unconstrained system and investigate (8) consisting merely of a terminal cost. We also provide a fixed final time  $t_f$ , as the velocity of this unconstrained system is not always bounded and the corresponding OC problems would otherwise not be well defined. In addition, we will mostly ignore the initial condition  $\mathbf{x}(0)$ , since the analytically obtained optimal strategies for our OC problems will not depend on  $\mathbf{x}(0)$ , as shown below.

Three different possibilities to excite the visco-elastic joint are investigated next, all of which assume a different motor model. These three different cases, which are summarized in Table I, will help interpret the system's optimal behaviour.

#### A. Velocity Source ( $u_1 = \dot{\theta}$ )

In this subsection, we assume that the motor dynamics of intrinsically elastic arms to be much faster than the link side dynamics. Consequently, we consider the motor to be a perfect velocity source<sup>2</sup>:  $u_1 = \dot{\theta}$ . Furthermore, we constrain the velocity of the motor  $u_1$  to be a piecewise continuous function and contained in the time-dependent set  $\mathbb{U}(t)$  described by two piecewise continuous functions  $u_{1min}(t)$  and  $u_{1max}(t)$ :

$$u_1(t) \in \mathbb{U}(t) = \{\bar{u} \in \mathbb{R} \mid u_{1min}(t) \leq \bar{u} \leq u_{1max}(t)\}, \quad (9)$$

such that constraints on the achievable motor velocities are being accounted for.

In order to apply the Minimum Principle, the dynamics of the model must be described in terms of first order differential equations. This can be done by defining the state vector to be  $\mathbf{x} = (\phi \quad \dot{q})^T$  and applying (6) with  $u_1 = \dot{\theta}$ . The

<sup>2</sup>The validity of the assumption may be shown by bringing the dynamics into singular perturbation form as done in [8].

first column of Table I summarizes the resulting equations  $\mathbf{f}$ . According to (3) the Hamiltonian  $\mathbb{H}$  becomes with  $L = 0$

$$\mathbb{H} = u_1(\lambda_1 + 2D\omega\lambda_2) - \lambda_1 x_2 + \omega^2 \lambda_2 x_1 - 2D\omega \lambda_2 x_2. \quad (10)$$

Applying the Minimum Principle (2) to (10), the optimal control  $u_1^*$  is known to depend on the sign of  $\sigma^*(t) = \lambda_1^*(t) + 2D\omega\lambda_2^*(t) = \lambda_1^* - \frac{2D}{\omega}\dot{\lambda}_1^*$ :

$$u_1^*(t) = \begin{cases} u_{1max}(t) & , \sigma^*(t) < 0 \\ u_{1min}(t) & , \sigma^*(t) > 0 \\ \text{singular} & , \sigma^*(t) = 0 \end{cases}, \quad (11)$$

where  $\sigma(t)$  is called the switching function. In order to compute the optimal controls, the sign of this function along time  $t$  needs to be determined.

By taking the partial derivative of (10) with respect to  $\mathbf{x}$  (see (4)), differential equations for the costates are obtained. The resulting equations are provided in Tab. I. Since these equations are autonomous and linear, boundary conditions are sufficient to uniquely determine the optimal costates  $\lambda^*$ . As no end constraints are present, (5) yields the missing boundary condition for the costates at final time  $t_f$ :

$$\lambda^*(t_f) = \frac{\delta \vartheta}{\delta \mathbf{x}} = \begin{pmatrix} 0 \\ -1 \end{pmatrix} \quad (12)$$

It is now possible to see that the costates are described by exactly the same mechanical system as the system states, see Fig. 1. Indeed, introducing the time transformation  $\tau = t_f - t$  with  $\tilde{\lambda}(\tau) := \lambda(t_f - t)$ , and rewriting the differential equations for the costates by taking the second time-derivative of the first costate in Tab. I, we arrive at the following well-known initial value problem [12]:

$$\tilde{\lambda}' = \begin{pmatrix} \omega^2 \tilde{\lambda}_2 \\ -\tilde{\lambda}_1 - 2D\omega \tilde{\lambda}_2 \end{pmatrix} \Rightarrow \tilde{\lambda}_1'' + 2D\omega \tilde{\lambda}_1' + \omega^2 \tilde{\lambda}_1 = 0, \quad (13)$$

where  $\omega^2 := \frac{K_J}{M}$ ,  $D := \frac{D_J}{2M\omega}$  and  $\frac{d\tilde{\lambda}}{d\tau} = \tilde{\lambda}' = -\dot{\lambda}$ . Thus, the dynamics of  $\tilde{\lambda}_1$  in (13) describe an unforced linear damped mass-spring system, with the same eigenfrequency  $\omega$  and damping ratio  $D$  as the robot joint (6). The initial conditions of this new system can be obtained from (12) and (13) as follows:

$$\begin{pmatrix} \tilde{\lambda}_1^*(0) \\ \tilde{\lambda}_1'^*(0) \end{pmatrix} = \begin{pmatrix} \lambda_1^*(t_f) \\ \omega^2 \lambda_2^*(t_f) \end{pmatrix} = \begin{pmatrix} 0 \\ -\omega^2 \end{pmatrix} \quad (14)$$

In order to obtain the optimal control  $u_1^*$ , (13)-(14) must be solved for  $\tilde{\lambda}_1^*$  such that the switching condition  $\sigma^* = \lambda_1^* - \frac{2D}{\omega}\dot{\lambda}_1^*$  can be obtained. Equation (13) is a linear second order differential equation with constant positive coefficients.

Damping Ratio, $D$	$u_1^*(t) = \dot{\theta}^*(t)$
$D = 0$	$\begin{cases} u_{1max}(t) \sin(\omega(t_f - t)) > 0 \\ u_{1min}(t) \sin(\omega(t_f - t)) < 0 \end{cases}$
$0 < D < 1$	$\begin{cases} u_{1max}(t) \cos(\omega_d(t_f - t) + \arctan \frac{2D^2 - 1}{2D\sqrt{1 - D^2}}) > 0 \\ u_{1min}(t) \cos(\omega_d(t_f - t) + \arctan \frac{2D^2 - 1}{2D\sqrt{1 - D^2}}) < 0 \end{cases}$
$D = 1$	$\begin{cases} u_{1max}(t) & t > t_f - \frac{2}{\omega} \\ u_{1min}(t) & t < t_f - \frac{2}{\omega} \end{cases}$
$D > 1$	$\begin{cases} u_{1max}(t) & t > t_f - \frac{\ln \frac{2D^2 - 1 + 2D\sqrt{D^2 - 1}}{2D^2 - 1 - 2D\sqrt{D^2 - 1}}}{2\omega\sqrt{D^2 - 1}} \\ u_{1min}(t) & t < t_f - \frac{\ln \frac{2D^2 - 1 + 2D\sqrt{D^2 - 1}}{2D^2 - 1 - 2D\sqrt{D^2 - 1}}}{2\omega\sqrt{D^2 - 1}} \end{cases}$

TABLE II: Optimal Control Strategies for  $u_1 = \dot{\theta}$

Thus, its solution depends not only on the initial conditions in (14), but also on its damping ratio  $D$  [12]. Indeed, depending on the magnitude of  $D$ , four different cases need to be considered. The computations for  $\lambda_1^*$  and  $\sigma^*$  are omitted for brevity. The corresponding optimal control strategies  $u_1^*$  are summarized in Tab. II. Let us briefly discuss these results.

a)  $D = 0$  (*Undamped System*): If the motor is attached to the link via a spring and no damping elements exist ( $D_J = 0$ ), (13) merely describes a mass oscillating with the joint eigenfrequency  $\omega = \sqrt{\frac{K_J}{M}}$ . Using the initial values in (14), we can derive

$$\sigma^*(t) = \lambda_1^*(t) = -\omega \sin(\omega(t_f - t)). \quad (15)$$

Equation (15) shows that the optimal costate  $\lambda_1^*$  never remains at zero for finite time. Furthermore, the switching condition (11) depends only on  $\lambda_1^*$ . Consequently, the optimal control  $u_1^*$  will always take its minimum or maximum values depending on the sign of  $\lambda_1^*$  as described in (11). Such a structure is called bang-bang control in literature [11], [13]. Note that  $u_1^*$  is periodic with  $\omega$ , as found already in [10].

b)  $0 < D < 1$  (*Underdamped System*): For  $D \in (0, 1)$ , the switching function  $\sigma^*$  can be written as

$$\begin{aligned} \Rightarrow \sigma^*(t) &= -\frac{\omega}{\sqrt{1 - D^2}} e^{-D\omega(t_f - t)} \cdot \cos\left(\omega_d(t_f - t) \right. \\ &\quad \left. + \arctan \frac{2D^2 - 1}{2D\sqrt{1 - D^2}}\right), \end{aligned} \quad (16)$$

where  $\omega_d = \omega\sqrt{1 - D^2}$  is the system's damped frequency. According to (16),  $\sigma^*$  oscillates with the damped eigenfrequency and its amplitude increases exponentially. Consequently, even if the robot link is connected to the motor with a damping element ( $0 < D < 1$ ), the optimal control  $u_1^*$  maximizing the end velocity  $\dot{q}(t_f)$  will be of bang-bang type. In particular, it oscillates with  $\omega_d$ .

c)  $D = 1$  (*Critically Damped System*): If  $D = 1$ , the switching function takes the form

$$\Rightarrow \sigma^*(t) = \omega^2 e^{-\omega(t_f - t)} \left(t_f - t - \frac{2}{\omega}\right). \quad (17)$$

According to (17), the switching function will switch its sign only once at  $t^* = t_f - \frac{2}{\omega}$  and remain negative for  $t > t^*$ . Consequently, if  $t_f$  is greater than  $\frac{2}{\omega}$ , the motor must start moving at its minimum velocity  $\dot{\theta}_{min}$  and then switch to its maximum velocity  $\dot{\theta}_{max}$  at  $t^* = t_f - \frac{2}{\omega}$ . The maximum link velocity is then obtained by letting the motor move with its maximum velocity  $\dot{\theta}_{max}(t)$  till final time  $t_f$  is reached.

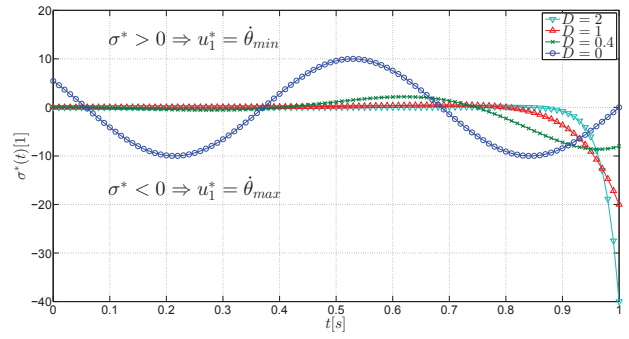


Fig. 2: Switching Function  $\sigma^*$  for  $u_1^* = \dot{\theta}$   
 $\omega = 10 \frac{rad}{s}, t_f = 1s$

d)  $D > 1$  (*Overdamped System*): If  $D > 1$ , the switching function takes the form:

$$\begin{aligned} \Rightarrow \sigma^*(t) &= 2D\omega e^{-D\omega(t_f - t)} \cdot \\ &\quad \left( \frac{2D^2 - 1}{2D\sqrt{D^2 - 1}} \sinh(\sqrt{(D^2 - 1)}\omega(t_f - t)) \right. \\ &\quad \left. - \cosh(\sqrt{(D^2 - 1)}\omega(t_f - t)) \right). \end{aligned} \quad (18)$$

As for the previous case, it is possible to show that the switching function  $\sigma^*$  in (18) will change its sign only once

at  $t^*(D) = t_f - \frac{\ln \frac{2D^2 - 1 + 2D\sqrt{D^2 - 1}}{2D^2 - 1 - 2D\sqrt{D^2 - 1}}}{2\omega\sqrt{D^2 - 1}}$  and remains negative for  $t > t^*$ . Consequently, if  $t_f > t^*$ , the optimal control strategy will be to first move at minimum velocity  $\dot{\theta}_{min}$  and then switch to  $\dot{\theta}_{max}$  at  $t = t^*$ . The motor velocity should then attain its maximum value  $\dot{\theta}_{max}(t)$  for all  $t \in (t^*, t_f]$ .

To sum up, the value of the damping ratio  $D$  plays a significant role for the optimal strategy to be followed. If the system is undamped or underdamped, the optimal motor velocity will switch periodically between its minimum and maximum values, where the period depends on the eigenfrequency  $\omega$  and the damped frequency  $\omega_d$ , respectively. On the other hand if  $D \geq 1$ , there is at most one switching from  $u_{1min}$  to  $u_{1max}$ . Fig. 2 illustrates the switching function  $\sigma^*$  for  $\omega = 10 \frac{rad}{s}, t_f = 1s$  and different damping ratios.

It is important to notice that the obtained optimal strategy is not easy to follow in a real system, when it involves switchings of the motor velocity. Indeed, switching the velocity instantaneously is only possible, if the motor experiences a mechanical impulse, which is in general not possible. Nevertheless, if the motor torque is high enough, it is still possible to make use of this optimal strategy by trying to minimize the duration needed to change the velocity from  $u_{1max}$  to  $u_{1min}$  and vice versa. This problem is addressed in [6], where it is shown that a bang-bang velocity control can be followed with little tracking error by choosing appropriate motor parameters, which then leads only to small deviations compared to the optimal solution.

#### B. Acceleration Source ( $u_1 = \ddot{\theta}$ )

Modeling the motor as a velocity source led to an optimal control strategy with a piecewise continuous motor velocity profile. Consequently, at points where the velocity is discontinuous, the magnitude of the torque needed to follow this profile tends to infinity. In order to obtain a continuous velocity profile, we now assume, that the motor acceleration

is directly controlled:  $u_1 = \ddot{\theta}$ . Furthermore, we constrain  $u_1$  to belong to the set  $\mathbb{U}(t)$  defined in (9), where  $u_{1min}$  and  $u_{1max}$  now denote the minimum and maximum achievable slope of the velocity profile.

To apply the Minimum Principle we again need first order differential equations, which can be obtained by extending the state vector of the previous model by a third state to  $\mathbf{x} = (\phi \quad \dot{q} \quad \dot{\theta})^T$  and noting that  $\dot{\phi} = x_3 - x_2$ . The resulting state-space representation is already given in Tab. I. Using this representation, the Hamiltonian  $\mathbb{H}$  becomes

$$\mathbb{H} = \lambda_1(x_3 - x_2) + \lambda_2(\omega^2 x_1 + 2D\omega(x_3 - x_2)) + \lambda_3 u_1. \quad (19)$$

According to the Minimum Principle, the optimal acceleration  $\ddot{\theta}^*$  will thus depend on the sign of  $\lambda_3^* = \sigma^*$  as follows:

$$u_1^*(t) = \begin{cases} u_{1max}(t) & , \lambda_3^* = \sigma^* < 0 \\ u_{1min}(t) & , \lambda_3^* = \sigma^* > 0 \\ \text{singular} & , \lambda_3^* = \sigma^* = 0 \end{cases} \quad (20)$$

Thus, in order to compute  $u_1^*$ , the third optimal costate needs to be found. The analytical expression for the costates can again be found by first obtaining their dynamics using (4) (see Tab. I) and then using the transversality condition (5), which yields the boundary conditions for  $\boldsymbol{\lambda}^*$  at  $t_f$ . In order to transform this problem into an initial value problem, we use again the time transformation  $\tau = t_f - t$  with  $\tilde{\boldsymbol{\lambda}}(\tau) := \boldsymbol{\lambda}(t_f - t)$  and obtain the following differential equations and initial values for the costates

$$\tilde{\boldsymbol{\lambda}}' = \begin{pmatrix} \omega^2 \tilde{\lambda}_2 \\ -\tilde{\lambda}_1 - 2D\omega \tilde{\lambda}_2 \\ \tilde{\lambda}_1 + 2D\omega \tilde{\lambda}_2 \end{pmatrix}, \quad \tilde{\boldsymbol{\lambda}}^*(0) = \begin{pmatrix} 0 \\ -1 \\ 0 \end{pmatrix}. \quad (21)$$

Note that the differential equations and the initial values of the first two costates  $\tilde{\lambda}_1^*$  and  $\tilde{\lambda}_2^*$  are exactly the same as the ones computed in the previous Section III-A (compare (21) with (12) and (13)). Consequently, these two costates remain the same. However, the optimal acceleration  $u_1^*$  now depends on  $\tilde{\lambda}_3^*$ . Nevertheless, a careful look at (21) shows that  $\tilde{\lambda}_3^*$  is related to  $\tilde{\lambda}_1^*$  as follows:

$$\begin{aligned} \tilde{\lambda}_3' &= -\tilde{\lambda}_2' \\ \Leftrightarrow \int_0^\tau \tilde{\lambda}_3' d\tau &= -\int_0^\tau \tilde{\lambda}_2' d\tau \\ \stackrel{(21)}{\Rightarrow} \tilde{\lambda}_3^*(\tau) &= -1 - \tilde{\lambda}_2^*(\tau) = -1 - \frac{\tilde{\lambda}_1^*}{\omega^2}, \end{aligned} \quad (22)$$

where the last equality is found using the first row of (21). Note that the solution for  $\tilde{\lambda}_1^*$  in (22) is already found for various damping ratios  $D$ , since  $\tilde{\lambda}_1^*$  did not change. Differentiating  $\tilde{\lambda}_1^*$  with respect to  $\tau$  and using (22) yields then the analytical expression for  $\tilde{\lambda}_3^*$ , on which the optimal control  $u_1^*$  depends. Table III summarizes these expressions for the new switching function  $\sigma^*(t) = \lambda_3^*(t) = \tilde{\lambda}_3^*(t_f - t)$  depending on  $D$ . Fig. 3 exemplifies its time evolution for  $\omega = 10 \frac{rad}{s}$  and different damping ratios.

As already mentioned, the analytical expressions for  $\lambda_3^*(t) = \tilde{\lambda}_3^*(t_f - t)$  in Tab. III depend on the magnitude of the damping ratios. For the undamped system,  $\lambda_3^*$  describes a harmonic oscillation around the equilibrium point  $-1$  with amplitude 1. In addition, for the damped robot joint ( $D > 0$ )  $\lambda_3^*$  is negative for all  $t \in [0, t_f)$  regardless the magnitude of  $D$ . Consequently,  $\lambda_3^*$  is never positive and never remains zero

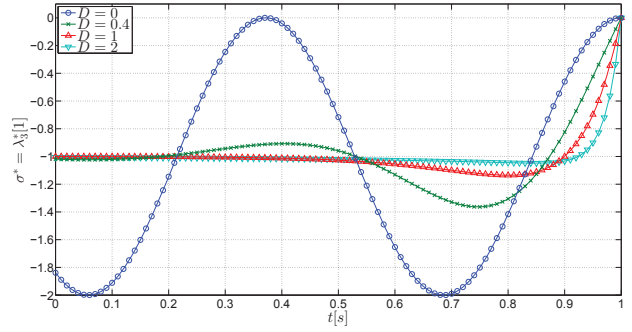


Fig. 3: Switching Function  $\sigma^*$  for  $u_1 = \ddot{\theta}$   
 $\omega = 10 \frac{rad}{s}$

for a finite time interval. According to (20), this means that the optimal motor acceleration of the robot link is always

$$\ddot{\theta}^*(t) = \ddot{\theta}_{max}(t). \quad (23)$$

According to the optimal strategy in (23), if  $\ddot{\theta}_{max}$  and  $t_f$  are large enough, the optimal strategy may lead to a violation of a possible constraint on the maximum motor velocity  $\dot{\theta}_{max}$  along this optimal trajectory. In order to account for this constraint, an OC Problem with state constraints must be solved ( $|x_3| \leq \dot{\theta}_{max}$ ). Such an OC Problem is not trivial to solve analytically, since the costates may be discontinuous and additional jump conditions need to be examined [13]. Numerical Simulations in Sec. IV will discuss the solution for this OC Problem in more detail.

### C. Torque Source ( $u_1 = \tau_m/B$ )

So far, we have not considered the dynamics of the motor and the resulting motor torques explicitly. In order to unveil the effect of the motor dynamics, we now consider a torque controlled motor such that in addition to (6), we also need to consider (7). Adding both equations and dividing the sum by  $B$  yields

$$\ddot{\theta} + \alpha \ddot{q} = \frac{\tau_m}{B} = u_1, \quad (24)$$

where  $\alpha := \frac{M}{B}$ . The control in (24) belongs to  $\mathbb{U}(t)$  in (9), where  $u_{1min}(t)$  and  $u_{1max}(t)$  now indicate the minimum and maximum achievable torques in  $t \in [0, t_f]$ . Defining the state vector as  $\mathbf{x} = (\phi \quad \dot{q} \quad \dot{\theta} + \alpha \dot{q})^T$ , the dynamics of the system can be described by first-order differential equations using (6) and (24), see Table I. The Hamiltonian for this OC Problem becomes

$$\begin{aligned} \mathbb{H} &= \boldsymbol{\lambda}^T \mathbf{f} \\ &= \lambda_1(x_3 - (\alpha + 1)x_2) \\ &\quad + \lambda_2(\omega^2 x_1 + 2D\omega(x_3 - (\alpha + 1)x_2)) + \lambda_3 u_1. \end{aligned} \quad (25)$$

According to (25),  $u_1^*$  depends on the sign of  $\lambda_3^*$  as in (20). Consequently, we again need to find the sign of  $\sigma^* = \lambda_3^*$  along the optimal trajectory. The dynamics of the corresponding costates are provided in Tab. I. The boundary condition for  $\boldsymbol{\lambda}^*(t_f)$  remains the same, since we still want to minimize the terminal cost  $\vartheta = -\dot{q}(t_f)$ . Using again the previous time transformation, we have the following initial

Damping Ratio $D$	$\lambda_3^*(t)$
$D = 0$	$-1 + \cos(\omega(t_f - t))$
$0 < D < 1$	$-1 + \frac{e^{-D\omega(t_f-t)}}{\sqrt{1-D^2}} \cos(\omega_d(t_f - t) + \arctan(\frac{D}{\sqrt{1-D^2}}))$
$D = 1$	$-1 + e^{-\omega(t_f-t)}(1 - \omega(t_f - t))$
$D > 1$	$-1 + e^{-D\omega(t_f-t)} \left( \cosh(\sqrt{(D^2-1)\omega(t_f-t)}) - \frac{D}{\sqrt{(D^2-1)}} \sinh(\sqrt{(D^2-1)\omega(t_f-t)}) \right)$

TABLE III: The Switching Function  $\sigma^* = \lambda_3^*$  for  $u_1 = \ddot{\theta}$

value problem:

$$\tilde{\lambda}' = \begin{pmatrix} \omega^2 \tilde{\lambda}_2 \\ -(\alpha+1)(\tilde{\lambda}_1 + 2D\omega \tilde{\lambda}_2) \\ \tilde{\lambda}_1 + 2D\omega \tilde{\lambda}_2 \end{pmatrix}, \tilde{\lambda}^*(0) = \begin{pmatrix} 0 \\ -1 \\ 0 \end{pmatrix} \quad (26)$$

According to (26),  $\tilde{\lambda}_3$  is related to  $\tilde{\lambda}_1$  as follows.

$$\begin{aligned} \tilde{\lambda}'_3 &= -\frac{1}{\alpha+1} \tilde{\lambda}'_2 \\ \stackrel{(26)}{\Rightarrow} \tilde{\lambda}^*_3(\tau) &= -\frac{1}{\alpha+1} \left( 1 + \frac{\tilde{\lambda}'_1}{\omega^2} \right) \end{aligned} \quad (27)$$

In order to compute  $\tilde{\lambda}_3^*$ , we investigate the already derived solution of  $\tilde{\lambda}_1$ . Indeed, differentiating the first row of (26) with respect to  $\tau$ , it can be seen that  $\tilde{\lambda}_1$  still describes a damped mass-spring system with the initial conditions from (14):

$$\begin{aligned} \tilde{\lambda}''_1 &= \omega^2 \tilde{\lambda}'_2 \\ &= -(\alpha+1)(\omega^2 \tilde{\lambda}_1 + 2D\omega \tilde{\lambda}'_1) \\ \Rightarrow \tilde{\lambda}''_1 + 2\bar{D}\bar{\omega} \tilde{\lambda}'_1 + \bar{\omega}^2 \tilde{\lambda}_1 &= 0, \end{aligned} \quad (28)$$

where  $\bar{\omega} = \sqrt{1+\alpha}\omega$  and  $\bar{D} = \sqrt{1+\alpha}D$ . Note that the eigenfrequency  $\bar{\omega}$  of this new system depends additionally on the motor mass  $B$  and is larger than  $\omega$ . Furthermore, the new damping ratio  $\bar{D}$  is greater than  $D$  as well. However, since the initial conditions are equal, equations for  $\tilde{\lambda}_1$  from the previous section can still be used to compute the first optimal costate by substituting  $\omega$  with  $\bar{\omega}$  and  $D$  with  $\bar{D}$ . With equation (27), one can then compute  $\lambda_3^*(t) = \tilde{\lambda}_3^*(t_f - t)$ , which now depends on the increased damping ratio  $\bar{D} = D\sqrt{1+\alpha}$ . The expressions from Tab. III can be used for  $\lambda_3^*$  in the torque controlled case, when the equations are scaled down by  $\frac{1}{\alpha+1}$  and  $D, \omega$  are replaced by  $\bar{D}, \bar{\omega}$  respectively.

In order to obtain the optimal torque  $\tau_m^* = Bu_1^*$ , we need to now find the sign of  $\lambda_3^*$  for different damping ratios  $\bar{D}$ . Since  $\lambda_3^*$  is only scaled by a constant positive factor, we can conclude that  $\lambda_3^*$  is never positive or never remains zero in a finite time-interval, similar to the third costate from the previous section. In other words, no matter how damped the robot link is, the optimal torque  $\tau_m^*$  maximizing the end-velocity is always the maximum achievable torque (see (20)):

$$\tau_m^*(t) = \tau_{m_{max}}^*(t). \quad (29)$$

Note that this strategy is likely to lead to a violation of the velocity constraint of the motor, if the magnitude of the maximal torque or  $t_f$  are sufficiently large.

For now, we discussed optimal control strategies for a damped flexible robot joint. The obtained strategies depend on the chosen motor model. If the motor is modeled as a pure velocity source, we see that for the undamped and

underdamped system, the optimal velocity is a periodic bang-bang control. On the other hand, for damping ratios  $D \geq 1$ , the motor velocity may switch only once from minimum to maximum velocity during the entire trajectory and this only if the final time is long enough. Otherwise, choosing the maximum velocity  $\dot{\theta}_{max}$  during the full trajectory maximizes the end velocity of the robot. Finally, if the acceleration of the motor  $\ddot{\theta}$  (or its torque  $\tau_m$ ) is directly controlled, the optimal strategy is to always apply the greatest control possible, no matter how damped the system is.

Note that, we have not explicitly stated an initial condition  $\mathbf{x}(0)$  for the models so far. Indeed, the derived strategies are valid for any given initial condition of the system since the dynamics and the boundary conditions of the costates do not depend on  $\mathbf{x}(t_0)$ . In the following Section III-D, we shortly discuss a useful interpretation of the costates, which will help us understand the different analytical expressions we derived for the costates. In particular, this interpretation is useful, if the optimal policies are to be implemented on a real elastic joint. It will also explain why the initial values of  $\mathbf{x}(t_0)$  do not have an influence on the optimal strategy.

#### D. Costates Interpretation

In this section, we provide an interpretation of the costates in terms of impulse response functions and discuss how one can make use of this. First, we exploit the linearity of the discussed models, describe their solutions using a convolution integral, and thus arrive at the relation between the system response to an arbitrary excitation and the system impulse responses. Applying then the Minimum Principle, the interpretation for the costates is provided.

A linear system can generally be described with first-order differential equations [2]

$$\dot{\mathbf{x}} = \mathbf{A}(t)\mathbf{x} + \mathbf{B}(t)\mathbf{u}, \quad (30)$$

where  $\mathbf{x} \in \mathbb{R}^n$  denotes the states of the system,  $\mathbf{u} \in \mathbb{R}^m$  the control vector,  $\mathbf{A} \in \mathbb{R}^{n \times n}$  the state matrix and  $\mathbf{B} \in \mathbb{R}^n$  the input matrix. Given an initial state  $\mathbf{x}(t_0)$ , the response of the state  $\mathbf{x}(t)$  to a control  $\mathbf{u}$  can then be written in terms of a convolution integral as follows [2].

$$\mathbf{x}(t) = \mathbf{G}(t, t_0)\mathbf{x}(t_0) + \int_{t_0}^t \mathbf{G}(t, \xi)\mathbf{B}\mathbf{u}(\xi) d\xi, \quad (31)$$

where  $\mathbf{G}(t, t_0)$  is the state-transition matrix. The state-transition matrix depends merely on the state matrix  $\mathbf{A}(t)$ , is unique, and satisfies

$$\frac{\partial \mathbf{G}(t, t_0)}{\partial t} = \mathbf{A}(t)\mathbf{G}(t, t_0), \quad \mathbf{G}(t_0, t_0) = \mathbf{I}. \quad (32)$$

$\mathbf{G}(t, t_0)$  can also be written as a matrix product:

$$\mathbf{G}(t, t_0) = \mathbf{U}(t)\mathbf{U}^{-1}(t_0), \quad (33)$$

where  $\mathbf{U}(t)$  is called the fundamental solution matrix, which satisfies  $\dot{\mathbf{U}}(t) = \mathbf{A}(t)\mathbf{U}(t)$  [2]. Furthermore, the terms in  $\mathbf{G}(t, t_0) = [g_{ij}(t, t_0)]_{i,j=1..n}$  provide the system impulse responses. Indeed,  $g_{ij}(t, t_0)$  yields the response of the  $i$ 'th state  $x_i(t)$  at  $t$  to a unit impulse function  $\delta(t - t_0)$  applied to the  $j$ 'th state at  $t_0$  [2]. Equation (31) thus shows how the system impulse response functions determine the way a given control trajectory  $\mathbf{u}$  affects the system state  $\mathbf{x}$ . Note that for fixed final time  $t_f$ , the influence of the initial state  $\mathbf{x}(t_0)$  on the obtained state  $\mathbf{x}(t_f)$  is given by  $\mathbf{G}(t_f, t_0)\mathbf{x}(t_0)$  and can not be influenced by the control  $\mathbf{u}$ , since  $\mathbf{G}(t_f, t_0)$  only depends on  $\mathbf{A}(t)$ . This justifies our previous statement that  $\mathbf{x}(t_0)$  does not influence the derived optimal strategies to maximize  $\dot{q}(t_f)$ .

As already mentioned, the response of a linear system to a control  $\mathbf{u}$  depends on the system state-transition matrix and thus on its impulse response functions. Consequently, there must exist a relation between the optimal control strategy and the system impulse responses. Indeed, the optimal costates  $\boldsymbol{\lambda}^*$  and the impulse response functions  $g_{ij}$  are closely related. To obtain this relation, we now look at the optimal control that maximizes a linear combination of the final states  $\boldsymbol{\alpha}^T \mathbf{x}(t_f)$  for the linear system (30):

$$J(\mathbf{u}) = \vartheta(t_f) = -\boldsymbol{\alpha}^T \mathbf{x}(t_f), \quad (34)$$

where  $\boldsymbol{\alpha} \in \mathbb{R}^n$  is a constant vector. Applying the Minimum Principle to the OC problem with the cost functional in (34), the Hamiltonian for the problem becomes:

$$\mathbb{H} = \boldsymbol{\lambda}^T \dot{\mathbf{x}} = \boldsymbol{\lambda}^T \mathbf{A}(t)\mathbf{x} + \boldsymbol{\lambda}^T \mathbf{B}(t)\mathbf{u}. \quad (35)$$

With this Hamiltonian, the costates can now be fully determined using (4), (5) and (32) as follows<sup>3</sup>:

$$\begin{aligned} \dot{\boldsymbol{\lambda}} &= -\frac{\partial \mathbb{H}}{\partial \mathbf{x}} = -\mathbf{A}^T(t)\boldsymbol{\lambda} \\ \boldsymbol{\lambda}^*(t_f) &= \frac{\partial \vartheta}{\partial \mathbf{x}} = -\boldsymbol{\alpha} \\ \Rightarrow \boldsymbol{\lambda}^*(t) &= -\mathbf{G}^T(t_f, t)\boldsymbol{\alpha}, \end{aligned} \quad (36)$$

where (36) finally provides the relation between the costates and the impulse responses  $g_{ij}$ , leading to the following interpretation: The  $j$ 'th costate  $\lambda_j^*(t)$  provides the response of the linear sum  $-\boldsymbol{\alpha}^T \mathbf{x}(t_f)$  at the final time  $t_f$  to the unit impulse function  $\delta$  applied to the  $j$ 'th state at  $t$ . To see this more clearly, one can rewrite equation (31) by premultiplying it with  $-\boldsymbol{\alpha}^T$  and evaluating it at  $t_f$ :

$$\begin{aligned} -\boldsymbol{\alpha}^T \mathbf{x}(t_f) &= -\boldsymbol{\alpha}^T \mathbf{G}(t_f, t_0)\mathbf{x}(t_0) \\ &\quad - \int_{t_0}^{t_f} \boldsymbol{\alpha}^T \mathbf{G}(t, \xi)\mathbf{B}\mathbf{u}(\xi) d\xi \\ \Leftrightarrow J(\mathbf{u}) &= \boldsymbol{\lambda}^{*T}(t_0)\mathbf{x}(t_0) + \int_{t_0}^{t_f} \boldsymbol{\lambda}^{*T} \mathbf{B}\mathbf{u} d\xi \end{aligned} \quad (37)$$

The  $j$ 'th costate  $\lambda_j(t)$  thus shows the influence of the control applied to the  $j$ 'th state on the cost functional  $J(\mathbf{u})$ <sup>4</sup>.

In order to appreciate the relation between the costates and the cost functional, let us now return to the elastic joint

<sup>3</sup>Note that  $\frac{\partial \mathbf{G}(t_f, t)}{\partial t} \stackrel{(33)}{=} \mathbf{U}(t_f) \frac{d\mathbf{U}^{-1}(t)}{dt} = -\mathbf{G}(t_f, t)\mathbf{A}(t)$

<sup>4</sup>Note that this interpretation of the costates is well-known in the general context of OC Theory, where for sufficiently smooth cost functionals the costates correspond to the partial derivative of the optimal cost  $J(\mathbf{u}^*)$  with respect to the system's initial state  $\mathbf{x}(t_0)$ , see for ex. [13].

model with its motor acting as a velocity source. Using (37), we can now write the following relation between the final velocity and the optimal costates<sup>5</sup>:

$$\begin{aligned} -\dot{q}(t_f) = -x_2(t_f) &= \lambda_1^*(t_0)x_1(t_0) + \lambda_2^*(t_0)x_2(t_0) \\ &\quad + \int_{t_0}^{t_f} (\lambda_1^* + 2D\omega\lambda_2^*)u_1 d\xi \end{aligned} \quad (38)$$

With equation (38), it is now obvious why the Minimum Principle in (11) must hold. In order to minimize  $-\dot{q}$ , the integral in (38) must be minimized. Consequently,  $u_1^*$  will depend on the sign of  $\sigma^* = \lambda_1^* + 2D\omega\lambda_2^*$  and always attain its maximum possible magnitude in order to maximize  $\dot{q}(t_f)$ . Similar arguments can also be made for the other two motor models, we analyzed. For the case, where the motor acceleration is directly controlled, we see for example:

$$\dot{q}(t_f) = -\boldsymbol{\lambda}^{*T}(t_0)\mathbf{x}(t_0) - \int_{t_0}^{t_f} \lambda_3^*(\xi)u_1(\xi) d\xi. \quad (39)$$

Since  $\lambda_3^*$  is always negative, the magnitude of the optimal costates  $|\lambda_3^*(t)|$  indicates how strong the achieved final velocity  $\dot{q}(t_f)$  depends on a control applied at  $t$ . For example, for the system illustrated in Fig. 3, if the system is overdamped ( $D = 2$ ), the effect of the control remains mostly the same until  $t \approx 0.9$ s and then decreases. On the other hand, if the system is undamped, a significant difference in the influence of the applied control  $u_1(t)$  on  $\dot{q}(t_f)$  along the trajectory can be observed. Nevertheless, since  $\lambda_3^*$  is always negative, the optimal control  $u_1^*$  remains the same for both cases.

Having now understood the relation between the minimized cost functional and the costates in terms of a convolution integral, we turn our attention in the following two subsections again to the motor velocity constraint  $|\dot{\theta}| < \dot{\theta}_{max}$ . Using (38) together with the analytical solutions from Section III-A, we first discuss the maximum performance limits of visco-elastic joints. We provide numerical results to discuss the effect of the motor velocity constraint on the optimal strategies (23) and (29), which were derived for the unconstrained system.

### E. Maximum Performance

In order to explicitly derive the performance of visco-elastic joints regarding explosive motions, we investigate the joint speed gain  $\epsilon = \frac{q_{max}}{\dot{\theta}_{max}}$ , assuming that the joint is initially at rest. In other words, we show how fast the link can move with respect to the maximum motor velocity, when it starts from its equilibrium  $\mathbf{x}(0) = \mathbf{0}$ .

Since we are interested in the maximum performance for a given motor velocity constraint, we model our motor as an ideal velocity source and ignore any other constraints. Consequently, we can make use of our results derived in Section III-A. According to the relation between the switching function and the cost functional in (38),  $\epsilon$  depends on  $t_f$  as follows.

$$\epsilon(t_f) = \frac{\max \dot{q}(t_f)}{\dot{\theta}_{max}} = \int_0^{t_f} |\sigma^*| dt, \quad (40)$$

where we used the fact that the optimal control is bang-bang with  $|u_1^*| = \dot{\theta}_{max}$ . We showed already that  $\sigma^*$  depends on the damping ratio (see (15)-(18)). Using the derived equations for  $\sigma^*$ , we can now calculate the integral in (40)

<sup>5</sup>Note that the control matrix for this case is simply  $\mathbf{B} = (1 \ 0)^T$ .

$\epsilon(n, D)$	$D = 0$	$D \in (0, 1)$	$D = 1$	$D > 1$
$n = 0$	2	$1 + F_1(D)$	$1 + e^{-2}$	$1 + F_2(D)$
$n = 1$	4	$1 + F_1(D) (2 + F_3(D))$	$1 + 2e^{-2}$	$1 + 2F_2(D)$
$n \geq 2$	$2(n + 1)$	$1 + 2F_1(D) \left( \sum_{i=0}^{n-1} F_3^i(D) + F_3(D)^n \right)$	–	–
$n \rightarrow \infty$	$\infty$	$1 + 2 \frac{F_1(D)}{1 - F_3(D)}$	–	–

$F_1(D) := e^{-\frac{D}{\sqrt{1-D^2}} \left( \pi - \arctan\left(\frac{2D\sqrt{1-D^2}}{1-2D^2}\right) \right)}$ ,  $F_2(D) := (2D^2 - 1 + 2D\sqrt{D^2 - 1})^{-\frac{D}{\sqrt{D^2 - 1}}}$ ,  $F_3(D) := e^{-\frac{\pi D}{\sqrt{1-D^2}}}$

TABLE IV: Maximum Performance  $\epsilon(D, n) = \frac{\dot{q}_{max}}{\theta_{max}}$  ( $u_1 = \dot{\theta}$ ,  $n =$  Switching Number of  $u_1^*$ ,  $\sigma^*(0) = 0$ )

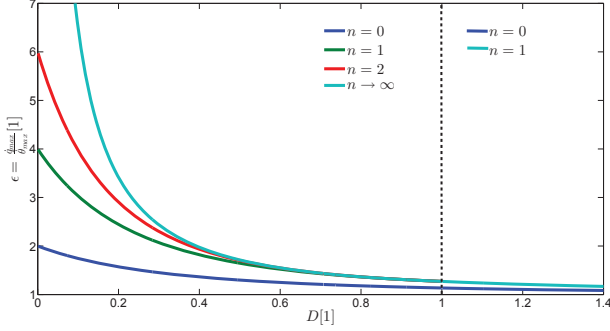


Fig. 4: Maximum Performance  $\epsilon(n, D) = \frac{\dot{q}_{max}}{\theta_{max}}$   $u_1 = \dot{\theta}$ ,  $n =$  Switching Number of  $u_1^*$ ,  $\sigma^*(0) = 0$

$\epsilon$	$D_J = 0$	$D_J = 0.4$	$D_J = 1$	$D_J = 2$
$u_1 = \dot{\theta}$	6.16	1.94	1.27	1.10
$u_1 = \ddot{\theta}$	5.85	1.90	1.26	1.09
$u_1 = \tau_m/B$	1.68	1.31	1.16	1.06

TABLE V:  $\epsilon = \frac{\dot{q}_{max}}{\theta_{max}}$  (Simulation Results)

and determine  $\epsilon$  as a function of  $D$  and  $t_f$ . These ratios are summarized in Table IV for a fixed switching number of  $u_1^*$  with  $\sigma^*(0) = 0$  and depicted in Fig. 4<sup>6</sup>,

It is important to note that  $\epsilon$  is bounded as soon as mechanical joint damping is present. We have shown in Sec. III-A that the link velocity of the damped joint can always be increased by enlarging  $t_f$ , and thus the switching number of  $u_1^*$ . Nevertheless, the presence of damping makes this increase bounded. Consequently, for high damping ratios, increasing  $t_f$  may have only little effect on the maximum velocity, and thus on  $\epsilon$ . For instance, if  $D$  is greater than 0.6, the change of  $\epsilon$  is neglectable for  $n > 1$ , see Fig. 4. It is also important to note that  $\epsilon$  in Tab. IV depends on  $D$ , but not on  $\omega$ . The eigenfrequency  $\omega$  determines only the switching instances (see Sec. III-A) and thus  $t_f$  at which  $\dot{q}_{max}$  is obtained.

In order to validate our theoretical results and to investigate the effect of the motor velocity constraint on the optimal velocity profiles, numerical results are presented next.

#### IV. NUMERICAL SIMULATIONS

In contrast to our previous discussions, the magnitude of the motor velocity will now be constrained in all the three models as follows.

$$(\forall t \in [t_0, t_f]) [|\dot{\theta}| < \dot{\theta}_{max} = \text{const.}] \quad (41)$$

<sup>6</sup>Note that given the switching number of  $u_1^*$ , the maximum value for  $\dot{q}$  and thus  $\epsilon$  is obtained when  $\sigma^*(0) = 0$ .

The system is again assumed to be at rest at  $t_0 = 0$  ( $x(0) = \mathbf{0}$ ) and the controls are bounded by:  $|u_1(t)| \leq u_{1max}$ . The constraint (41) can cause different control strategies compared to (23) and (29).

The numerical computations were obtained with the software GPOPS[14], which uses the Gauss Pseudospectral Method to solve OC Problems ([1], [3]). Figure 5 (left row) visualizes the obtained motor velocities of the three different models for different damping ratios, while the obtained performance is summarized in Tab. V. The optimal switching function  $\sigma^*$  in (15)-(18), which determines the optimal velocity profile for the model in Sec. III-A is depicted as well. Even though  $\sigma^*$  only determines the switching strategy for this model, it relates the motor velocity  $\dot{\theta}$  and the final link velocity  $\dot{q}(t_f)$  regardless of the chosen motor control. Indeed, for all the three considered models, the force acting on the link is due to the elastic joint torque and the viscous damping, which depend on the positions and velocities of motor and link, respectively. The impulse-response function, relating the velocity of the motor to the link is thus valid for all three models and using the convolution integral in (38) with  $x(0) = \mathbf{0}$ , we can obtain the following relation for all considered motor models ( $x(0) = \mathbf{0}$ ).

$$\dot{q}(t_f) = - \int_0^{t_f} \sigma^*(\xi) \dot{\theta}(\xi) d\xi \quad (42)$$

According to (42), the switching function  $\sigma^*(t)$  at  $t$  describes the influence of the motor velocity  $\dot{\theta}(t)$  at time  $t$  on  $\dot{q}(t_f)$ . With this information the optimal velocity profile for  $u_1^* = \dot{\theta}$ , which is illustrated in Fig. 5, can easily be interpreted: the optimal acceleration  $\ddot{\theta}(t)$  switches whenever the influence  $|\sigma^*(t)|$  approaches zero. Consequently, the difference in the achieved final link velocities differ not significantly (right row in Fig. 5). Furthermore, depending on the system damping, the switching times and structure change. Indeed, for the undamped case ( $D = 0$ ), we see that there is a certain symmetry in the two velocity profiles for  $u_1^* = \dot{\theta}^*$  and  $u_1^* = \ddot{\theta}^*$ . To be more specific, the velocity of the motor, whose acceleration is optimally controlled, reaches zero whenever  $\sigma^*$  is zero. This is due to the fact that  $\sigma^*$  describes a harmonic motion. For the under-damped case, on the other hand, the amplitude of  $\sigma^*$  is increasing and this symmetry is lost. Similar observations can also be made for  $D \geq 1$ .

We have thus seen that the switching function  $\sigma^*(t)$  and the convolution integral (42) can be used to interpret the optimal system behaviour. Nevertheless, care must be taken when this approach is followed, since merely looking at (42) might lead to false conclusions. For instance, if we compare the velocity profile of the torque controlled motor with the switching function, a direct relation does not seem to exist if the system is undamped ( $D = 0$ ). Indeed, for the

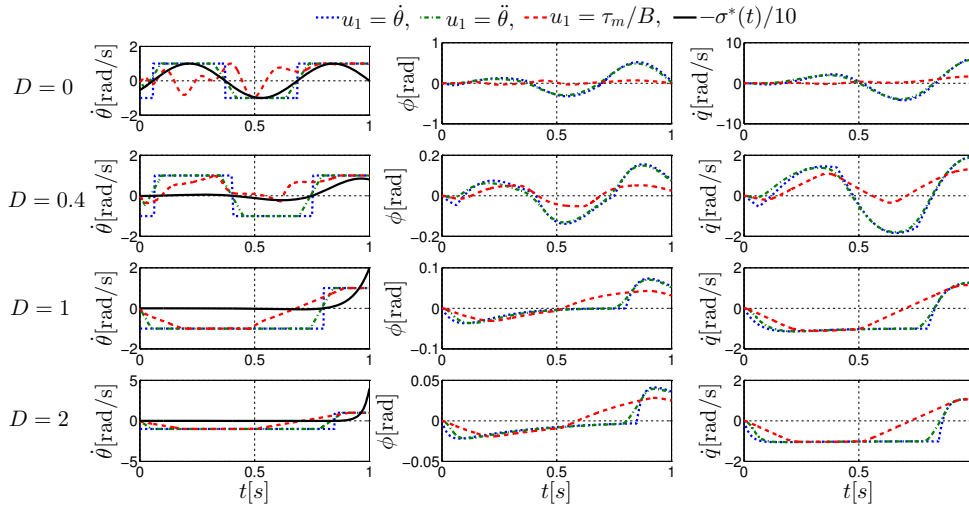


Fig. 5: Simulation results for  $|\dot{\theta}| \leq 1 \frac{\text{rad}}{\text{s}}$   
 $x(0) = \mathbf{0}, \omega = 10 \frac{\text{rad}}{\text{s}}, \alpha=3, \ddot{\theta}_{max} = -\ddot{\theta}_{min} = 20 \frac{\text{rad}}{\text{s}^2}, \frac{\tau_{m,max}}{B} = -\frac{\tau_{m,min}}{B} = 20 \frac{\text{rad}}{\text{s}^2}$

torque controlled motor, the constraint in (41) also affects the maximum angular deflection achievable by the system. A very high deflection might lead to the violation of the constraint in the motor velocity, if the torque is not high enough to brake the motor. Consequently, as seen in Fig. 5 (middle row), the angular deflection  $\phi$  obtained with the torque controlled motor model is considerably smaller compared to the other two models, resulting also to smaller  $\epsilon$ , see Tab. V). As damping increases, this effect on the angular deflection is not as crucial. Consequently, the three velocity trajectories resemble each other and the difference in  $\epsilon$  become smaller, see Tab. V.

## V. CONCLUSION

In this paper we gave several insights into the optimal control of visco-elastic joints with different motor models and discussed especially the influence of constant mechanical joint damping on the optimal control policy regarding explosive motions. Having established the relation between the system's costates and impulse response functions for general time-varying linear systems, we showed how this property can be used in interpreting numerical simulation results and how additional state constraints might effect the resulting strategy.

Despite we mainly focused on explosive motions, many other motion types exist that can be investigated with OC theory to elaborate how to fully exploit elastic system's dynamics. The problem is rather new in robotics with many interesting open questions to be treated in the future. Our ongoing research focuses on addressing these questions for 1-DoF joints, including variable stiffness joints [7], and extending the obtained results to systems with state constraints, non-linear spring characteristics and finally to  $n$ -DoF systems with non-linear dynamics. Our first results into this direction can be found in [10], [8], [7].

## ACKNOWLEDGMENT

This work has been partially funded by the European Commission's Sixth Framework Programme as part of the project SAPHARI under grant no. 287513.

## REFERENCES

- [1] David Benson. *A Gauss Pseudospectral Transcription for Optimal Control*. PhD thesis, Massachusetts Institute of Technology, Department of Aeronautics and Astronautics, 2005.
- [2] C.T. Chen. *Linear System Theory and Design*. Oxford University Press, 2009.
- [3] Divya Garg, Michael A. Patterson, William W. Hager, Anil V. Rao, David A. Benson, and Geoffrey T. Huntington. A unified framework for the numerical solution of optimal control problems using pseudospectral methods. *Automatica*, 46(11):1843–1851, 2010.
- [4] Markus Grebenstein, Alin Albu-Schäffer, Thomas Bahls, Maxime Chalon, Oliver Eiberger, Werner Friedl, Robin Gruber, Sami Haddadin, Ulrich Hagn, Robert Haslinger, Hannes Hoppner, Stefan Jörg, Mathias Nickl, Alexander Nothhelfer, Florian Petit, Josef Reill, Nikolaus Seitz, Thomas Wimböck, Sebastian Wolf, Tilo Wusthoff, and Gerd Hirzinger. The DLR hand arm system. pages 3175–3182, 2011.
- [5] S. Haddadin, K. Krieger, N. Mansfeld, and A. Albu-Schaffer. On impact decoupling properties of elastic robots and time optimal velocity maximization on joint level. In *Intelligent Robots and Systems (IROS), 2012 IEEE/RSJ International Conference on*, pages 5089–5096, 2012.
- [6] S. Haddadin, N. Mansfeld, and A. Albu-Schaffer. Rigid vs. elastic actuation: Requirements amp; performance. In *Intelligent Robots and Systems (IROS), 2012 IEEE/RSJ International Conference on*, pages 5097–5104, 2012.
- [7] S. Haddadin, M.C. Özpapucu, and A.A. Schäffer. Optimal control for maximizing potential energy in variable stiffness joints. In *Proc. 51st IEEE Conf. Decision and Control (CDC)*, Maui, HI, USA, 2012.
- [8] Sami Haddadin, Felix Huber, and Alin Albu-Schäffer. Optimal control for exploiting the natural dynamics of variable stiffness robots. In *ICRA*, pages 3347–3354, 2012.
- [9] Sami Haddadin, Tim Laue, Udo Frese, Sebastian Wolf, Alin Albu-Schäffer, and Gerd Hirzinger. Kick it with elasticity: Requirements for 2050. *Robotics and Autonomous Systems*, 57:761–775, 2009.
- [10] Sami Haddadin, Michael Weis, Alin Albu-Schäffer, and Sebastian Wolf. Optimal control for maximizing link velocity of robotic variable stiffness joints. In: *Proceedings. IFAC 2011, World Congress*, pages 3175–3182, 2011.
- [11] D. Liberzon. *Calculus of Variations and Optimal Control Theory: A Concise Introduction*. Princeton University Press, 2011.
- [12] L. Meirovitch. *Principles and techniques of vibrations*. Prentice Hall, 1997.
- [13] M. Papageorgiou. *Optimierung: Statische, dynamische, stochastische Verfahren*. Oldenbourg, 1996.
- [14] Anil V. Rao, David A. Benson, Christopher Darby, Michael A. Patterson, Camila Francolin, Ilyssa Sanders, and Geoffrey T. Huntington. Algorithm 902: Gpops, a matlab software for solving multiple-phase optimal control problems using the gauss pseudospectral method. *ACM Trans. Math. Softw.*, 37:22:1–22:39, April 2010.
- [15] Ronald van Ham, Thomas Sugar, Bram Vanderborgth, Kevin Hollander, and Dirk Lefeber. Compliant actuator designs: Review of actuators with passive adjustable compliance/controllable stiffness for robotic applications. *IEEE Robotics and Automation Mag.*, 16(3):81–94, 2009.